ETH ZÜRICH

Same-sign dileptons as a search tool at CMS

Author:
Marc Dünser

Supervisor:
Prof. Dr. Rainer Wallny

A thesis submitted in fulfilment of the requirements
for the degree of Doctor of Science

in the

Institute for Particle Physics
D-PHYS

December 2014

Declaration of Authorship

I, Marc Dünser, declare that this thesis titled, 'Same-sign dileptons as a search tool at CMS' and the work presented in it are my own. I confirm that:

- This work was done wholly or mainly while in candidature for a research degree at this University.

- Where any part of this thesis has previously been submitted for a degree or any other qualification at this University or any other institution, this has been clearly stated.

- Where I have consulted the published work of others, this is always clearly attributed.

- Where I have quoted from the work of others, the source is always given. With the exception of such quotations, this thesis is entirely my own work.

- I have acknowledged all main sources of help.

- Where the thesis is based on work done by myself jointly with others, I have made clear exactly what was done by others and what I have contributed myself.

Signed:

Date:

"The White Rabbit put on his spectacles. 'Where shall I begin, please your Majesty?' he asked. 'Begin at the beginning,' the King said gravely, 'and go on till you come to the end: then stop.'"

Alice in Wonderland

ETH ZÜRICH

Abstract

Faculty Name

D-PHYS

Doctor of Science

Same-sign dileptons as a search tool at CMS

by Marc Dünser

The Thesis Abstract is written here (and usually kept to just this page). The page is kept centered vertically so can expand into the blank space above the title too...

For/Dedicated to/To my...

Contents

Chapter 1

Introduction

The construction of the Large Hadron Collider (LHC) and its experiments at CERN in Geneva over the few last decades has been just the last step in a long and successful history of particle accelerators that started roughly 100 years ago. Just as the first specimens of its kind, the LHC serves – first and foremost – the purpose of fundamental research. It has been conceived in order to answer some of the most fundamental questions of modern day physics, such as *'how do particles acquire mass?'* or *'what is dark matter?'*. Despite the purely scientific origin of these questions and the improbability of any 'practical' application from any possible answer to them, it is important to note that fundamental research in general and the research at the LHC in particular do serve a greater and more applicable purpose.

The invention of the world wide web and HTML FIXME(CITE), early developments on touch screens, research on medical physics with high-power magnet systems as well as medical imaging and the use of high energy ion beams for tumor treatment are only a few examples of the direct consequences on daily life which fundamental research on particle physics entails.

This thesis is dedicated almost exclusively to data analysis of high-energy particle collisions which took place in the CMS experiment at the LHC. By looking at such collisions, the aforementioned question about the origin of mass has already been answered FIXME(CITE) with the discovery of the Higgs boson in 2012 by both the CMS and ATLAS collaborations. The second question, however, remains unanswered and the work presented in the following is largely devoted to a search for particles which could provide physicists with a suitable candidate for a dark-matter particle.

Chapter 2 describes the fundamentals of particle physics from a theoretical standpoint, Chapter FIXME will provide on overview of the CMS experiment. Chapters FIXME to FIXME will then describe the search for new physics etc. blabla.

Chapter 2

Theory

In order to interpret any experimental result, it is of paramount importance to understand the underlying model governing the physical processes in question. Modern physics knows a large number of rather successful theories all dedicated to describing different mass and energy scales. An example is the theory of classical mechanics, which manages to describe the physics of 'daily life' very well. However, it breaks down when velocities approach the speed of light and has to be incorporated into a broader theory, namely that of relativity.

This specific example already suggests that different physical theories are valid only in a certain energy range and describe only a certain 'type'[1] of physical process. This fact is also true for the case of particle physics. The relevant theory is called the *'Standard Model'* and will be described hereafter. Further into the chapter, a short description of the pitfalls of the standard model will be given with some explanation on possible solutions.

2.1 The Standard Model

The Standard Model (SM) of particle physics provides the theoretical framework that describes all fundamental particles and the forces that act between them, with the one exception of gravity. Despite a few drawbacks that will be described later (see Section 2.1.3) it has been an overwhelmingly successful theory, capable of describing experimental data with a precision that is simply outstanding.

---

[1]In this particular example electromagnetic interactions are – for instance – not described at all.

Chapter 3

Experimental Setup

All data analysed in this thesis was recorded with the CMS experiment at the Large Hadron Collider (LHC) at the European Organization for Nuclear Research (CERN) near Geneva, Switzerland. This chapter provides a short overview of CERN and its accelerators, the LHC, as well as a short description of the main hardware components of the CMS experiment.

3.1 The Large Hadron Collider

The LHC [1] is currently by far the largest and most powerful particle accelerator in the world. It is a circular accelerator situated in a tunnel around 100 metres below the Swiss-French border west of Geneva. Its main purpose is accelerating protons to energies of up to 13 TeV [1] in the final development stage of the machine starting in 2015. Besides the acceleration of protons it is also capable of accelerating heavy ions (predominantly lead ions) to energies of up to 2.76 TeV per nucleon.

3.1.1 The acceleration chain

Particles injected into the LHC for final acceleration are required to have an energy of 450 GeV. This is achieved by a long chain of linear and circular accelerators, a sketch of which can be seen in Fig. 3.1.

Protons used for acceleration in the LHC are extracted from a hydrogen molecules in a bottle situated at the CERN main site. These molecules are stripped of their electrons

---

[1]One electronvolt (eV) is the energy acquired by a charge of $1e$ passing through an electric field of 1 volt, equivalent to 1.602×10^{-19} Joule.
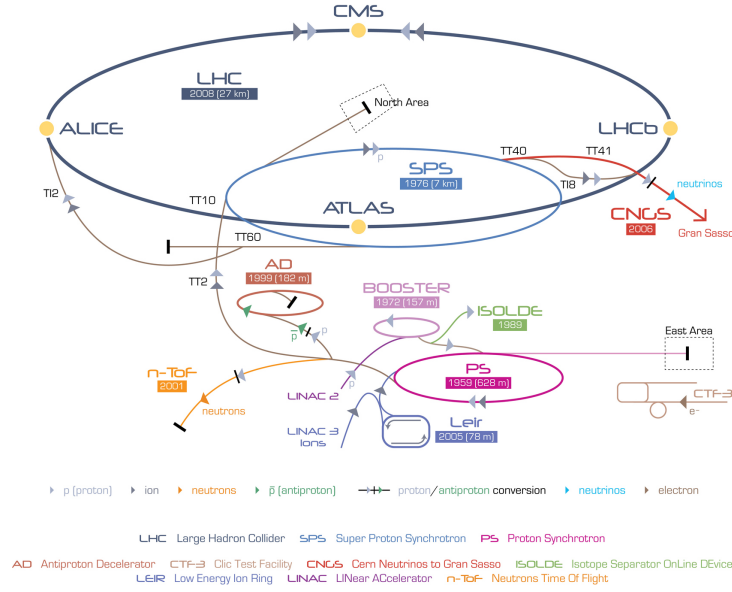
FIGURE 3.1: Conceptual drawing of all accelerators and experiments hosted at CERN. Besides operating the LHC, there are many other accelerators, decelerators and experiments being operated.

by strong electric fields and subsequently injected into the first acceleration stage, the linear accelerator Linac 2. Upon exiting Linac 2, the protons have gained an energy of 50 MeV and are injected into the first circular accelerator, the Booster. This synchrotron with a circumference of 157 meters accelerates the protons to an energy of 1.4 GeV and uses magnetic dipole fields to bend the protons onto a circular path. These bending magnets are operated at room temperature for the Booster and in fact all the accelerators up to the LHC. From the Booster, the protons are injected further into the Proton Synchrotron, an accelerator originally built in 1959 with a circumference of 628 meters and an output energy of 25 GeV. The last step before injection into the LHC is the Super Proton Synchrotron (SPS), which accelerates the protons to the LHC injection energy of 450 GeV. The SPS is the world's second largest accelerator with a circumference of nearly 7 km, and it was the first accelerator to collide protons and anti-protons at energies high enough to produce *W* and *Z* bosons, leading to their discovery in 1983 [2, 3].

Ions pass through the same accelerators on their way to the LHC with the notable exception of the very first acceleration being done in Linac 3 rather than Linac 2.

While the LHC is filled and delivering collisions to its experiments, the accelerators are used to provide particles to other experiments ongoing at CERN. The Antiproton Decelerator (AD) in which anti-protons are decelerated and combined with positrons to form anti-hydrogen, and the ISOLDE collaboration for the study of many different radioactive ions are just some of the examples of interesting experiments ongoing at CERN.

3.1.2 Specifications of the LHC

The LHC itself is located in a tunnel roughly 50-150 meters below ground in the Geneva area, extending from Lake Geneva all the way to the Jura mountain chain. Its total circumference is 26 659 meters which makes it – together with its predecessor the Large Electron Positron Collider hosted in the same tunnel – by far the largest particle accelerator ever built. It is divided into 8 sectors, separated and named by the eight access points to the tunnel. A schematic drawing of the LHC with all its access points can be found in Fig. 3.2. Access points 1, 2, 5, and 8 host the four main experiments ATLAS, ALICE, CMS, and LHCb, the acceleration is performed by radio-frequency (RF) cavities at point 4, the beam-dump system is located at point 6 and beam monitoring and conditioning is performed at points 3 and 7 [4].
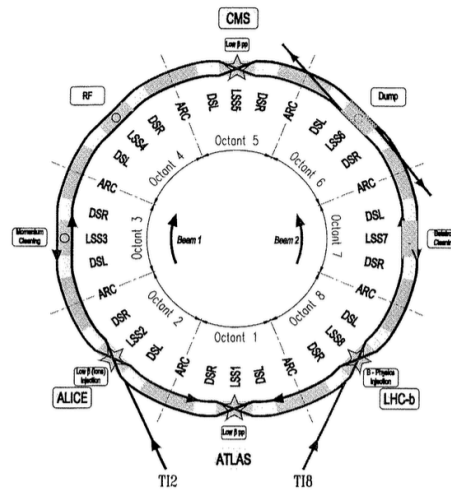
FIGURE 3.2: Schematic drawing of the LHC ring and its sectors and access points numbered in clockwise direction starting at the ATLAS experiment in point 1.

The magnet system

Particles are injected from the SPS into the LHC into two counter-rotating beams in discrete bunches at the aforementioned 450 GeV. In order to control the particles on their circular path, an intricate magnet system was designed in order to bend and to focus the beams. The main feature of the LHC magnet system are the 1232 dipole bending magnets, each roughly 15 meters in length and weighing 30 tonnes. These magnets are made of a niobium-titanium alloy, a type-2 superconductor which allows current transport without loss at the operating temperature of 1.9 K. Cooling of the LHC cold mass of roughly 37 Mt is achieved with pressurized superfluid helium. Each magnet hosts two separate beam-pipes for beam 1 (clockwise) and beam 2 (counter-clockwise)

with the dipole magnetic field pointing in opposite direction in either of them. In or-
der to achieve acceptable beam lifetimes and to minimize beam-gas interactions, the
beam pipes are evacuated and the residual gas pressure is around 10^{-10} mbar. Upon
injection from the SPS the dipole magnets are operated at a magnetic field strength of
0.535 T which is slowly raised during the acceleration period of the beam to a final field
strength of 8.33 T at the maximum collision energy.

Alongside the dipole magnets for the bending of the particles, there are thousands of
additional magnets for correcting and controlling the particle's path. The largest part
of the correction magnets are sextupole magnets situated on either side of every dipole
magnet. Further components include a decapole and an octupole corrector for each
dipole magnet as well as injection kicker magnets and kicker magnets for the beam
dump system among others.

The RF cavities

Once the LHC is filled and circulation of the beams is stable, they are accelerated from
their initial energy by the means of so-called RF cavities which provide a high fre-
quency alternating electric field of nominally 400.8 MHz. Similar to the bending mag-
nets, the RF cavities are operated in a superconducting state at a temperature of 1.9 K.
There are a total of eight such cavities per beam, each achieving a potential difference
of 2 MV for a combined 16 MV necessary for acceleration at collision energy. During
the acceleration period of the beams, the energy gain per particle per turn is 485 keV
with the total power consumption of the RF system being around 275 kW.

Beam parameters

In order to measure the performance of a particle accelerator such as the LHC, the
quantities of instantaneous and integrated luminosity are the most important figure of
merit, as they correspond to the total number of particle collisions produced in any
given collision point. The instantaneous luminosity is defined as

$$L = \frac{N_b^2 n_b f_{rev} \gamma_r}{4\pi\epsilon_n\beta^*}F, \tag{3.1}$$

where N_b denotes the number of particles per bunch, n_b the number of bunches per
beam, f_{rev} the revolution frequency of each bunch, γ_r the relativistic gamma factor, ϵ_n
the normalized beam emittance, β^* the β-function of the beam at the collision point, and

TABLE 3.1: Beam parameters for beams in the LHC at injection and collision energy.

Beam parameters			
	Unit	Injection	Collision
Beam Energy	[GeV]	450	3500 - 7000
Relativistic γ_r		479.6	3730-7461
Particles per bunch		1.15×10^{11}	
No. of bunches		2808	
f_{rev}	[Hz]	11245	
ϵ_n	[μm rad]	3.5	3.75
Half crossing angle[2]	[μrad]	$\pm$ 160	$\pm$ 142.5
β^*	[m]	18	0.55

F a geometrical factor inversely proportional to the crossing angle of the two beams at the interaction point.

The beam emittance is defined as the volume of the beam in the position-momentum phase space and is thus a measure of the quality of the beam. Emittance itself is inversely proportional to the beam momentum and it is therefore necessary to introduce a normalized emittance, which does not change its value with momentum in order to compare beam quality before and after acceleration. The β-function describes the behavior of the transverse beam size as a function of the position in the accelerator, and the value β^* is consequently proportional to the transverse size of the beam at the collision point.

The dimension of the instantaneous luminosity is $cm^{-2}s^{-1}$ and by integrating it over time the integrated luminosity $\mathcal{L}_{int}$ is obtained. Through knowledge of the latter, one can calculate the total number of expected events for any given physical process in a data sample of a given size by

$$N_{\text{process}} = \mathcal{L}_{int} \cdot \sigma_{\text{process}}. \tag{3.2}$$

All relevant beam parameters to calculate the instantaneous luminosity at the LHC are summarized in Table 3.1 at both injection and collision energies.

Performance of the LHC

All values in Table 3.1 refer to the design values of the LHC, while the actual performance since startup in 2008 has been considerably different. After the initial startup in the autumn of 2008 when beams were first injected into the machine, a faulty connector between superconductors caused a significant explosion in the cooling system of the

main magnets, resulting in a shutdown and repair period until late 2009. However, upon restarting of the machine in 2009, operations of the LHC have been almost flawless, with many parameters of the LHC reaching or even exceeding their design targets. Since the limiting factor for the LHC energy is the attainable magnetic field strength in the bending magnet, combined with safety concerns regarding the replaced connectors from the incident in 2008, a staged approach for a slow energy ramp-up was implemented for the LHC. First stable collisions for data-taking in 2010 were performed at an energy per proton of 3.5 TeV resulting in 7 TeV center-of-mass energy. This energy was maintained also during 2011 before being increased to 8 TeV in center-of-mass energy during the 2012 data-taking period. This thesis focuses on the dataset at 8 TeV. The energy will further be increased to 13 TeV in center-of-mass in early 2015.

Regarding the luminosity, the LHC has outperformed its early expectations. Despite the fact that so far only half the bunches were filled, resulting in a bunch spacing of 50 ns instead of the design 25 ns, the maximum instantaneous luminosity has almost reached its design value of $1 \times 10^{34} \ cm^{-2}s^{-1}$ in late 2012, when an LHC fill with an instantaneous luminosity of $7.67 \times 10^{33} \ cm^{-2}s^{-1}$ was recorded. This was mostly due to the increase in protons per bunch.

Pileup

In order to reach the luminosities discussed in the previous section, it is necessary for the LHC to produce more than one proton-proton collision per bunch crossing in the experiments. This effect is called pileup and poses great difficulty to the experiments in handling the many interaction vertices. Since the total inelastic cross-section in the LHC is dominated by rather unexciting, low-mass and low-energy very forward QCD interactions, it is very unlikely to observe more than one 'interesting' proton-proton collision per bunch crossing. Nevertheless, some problems for the experiments associated with pileup include the identification of the 'interesting' vertex, the assignment of electrically neutral particles to said vertex, energy corrections for detector objects such as jets, leptons, and the missing momentum due to pileup interactions, and occupancy in the subdetectors.

The number of proton-proton interactions per bunch crossing follow a Poisson-distribution of which the mean reached about 20 in 2012 [5].

3.2 The CMS experiment

As briefly mentioned before, the LHC provides high energy particle collisions to four large particle physics experiments, namely the ALICE, ATLAS, CMS, and LHCb experiments. While the ALICE and LHCb experiments are specially designed for specific purposes, the study of heavy ion collisions and the study of processes involving the b-quark, respectively, the ATLAS and CMS experiments are design as 'general purpose' experiments. As such, their goal is the detailed scrutiny of the SM, the search for the recently observed Higgs boson [FIXME - reference], and the search for new physics phenomena. They do this by means of measuring and absorbing decay products of the collisions. The relevant physical observables of any particle produced in a particle collisions are the momentum vector and the energy of a particle. Once these two quantities are known, every particle can be identified unambiguously.

Data collected for this thesis were recorded by the CMS experiment.

3.2.1 General structure and the magnet

The Compact Muon Solenoid (CMS) experiment is located roughly 100 meters below ground in Cessy, France, it is cylindrically shaped with dimensions of roughly 22 meters in length and a diameter of about 16 meters. The whole apparatus comprises a barrel part in the center and a so-called endcap on either side to seal the detector as hermetically as possible. A drawing of the CMS detector is shown in Fig. 3.3.

The convention for the coordinate system is as follows. The origin of the coordinate system is at the nominal interaction point. The x-axis points towards the center of the LHC ring, the y-axis points towards the surface and the z-axis points towards the west, along beam 2. The azimuthal angle ϕ is measured in the x-y plane, while the polar angle θ is measured from the positive z-direction. It is commonly replaced by a quantity called pseudo-rapidity defined as $\eta = -\log\left[\tan\left(\frac{\theta}{2}\right)\right]$.

As the presence of the word 'solenoid' in the acronym for CMS already suggests, its main feature is a very large, solenoid magnet which defines the overall structure of the experiment. Much like the LHC bending magnets, it is a superconducting structure and the conducting material is a niobium-titanium alloy, albeit at a very different scale. It measures roughly six meters in inner diameter and 13 meters in length, carrying a current of about 18 000 (FIXME) ampere, resulting in a maximum magnetic field strength of 3.8 T [6]. In addition to the actual magnet, the CMS magnet system also comprises a return yoke for the magnetic field lines to be homogeneous as a function of the distance from the interaction point. Altogether, the magnet system weighs approximately 11 000
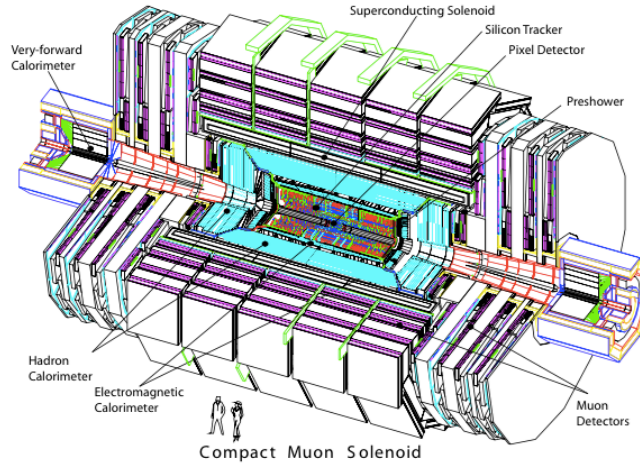
FIGURE 3.3: Perspective view of the CMS detector. The cylindrical shape as well as the barrel and endcap geometry can be clearly seen. The depicted people are to scale [4].

metric tons, by far the heaviest component of the CMS detector. As momentum resolution of charged particles is a critical factor in the physics performance of a detector, the magnetic field strength within the tracking volume is desired to be as large as possible.

The large volume of the CMS magnet allows for most sub-detectors to be situated within a very high magnetic field. Not only the tracking detectors, but also the calorimetry for energy measurement are fully incorporated within the magnet's volume.

3.2.2 The sub-detectors

The structure of CMS is a layered, onion-like assembly of different sub-detectors. In the very center, the beryllium beam-pipe passes through the detector with a diameter of 2.5 cm FIXME!!. Moving radially outwards from the center of the beam-pipe, the layers are first the silicon pixel detector followed by the silicon strip tracker, the electromagnetic calorimeter, the hadronic calorimeter, the superconducting magnet and finally the magnet return yoke interleaved with the muon chambers.

The CMS pixel detector

The CMS pixel detector is a layered silicon detector with a pixel size of $100 \times 150 \; \mu m^2$ with the purpose of measuring the trajectory of charged particles very precisely. It

is divided into a barrel (BPIX) and two endcap 'forward' parts (FPIX) symmetrically arranged around the nominal interaction point. The BPIX comprises three concentric layers of 53 cm in length and at radii of 4.3, 7.2, and 11 cm from the interaction point, while there are two FPIX disks on either side of the BPIX, at distances of z=±34.5 and z=±46.5 cm, extending from a radius of 6 to 15 cm. In combination, the barrel and endcap part provide high granularity tracking up to a pseudo-rapidity of η = 2.5, corresponding to a polar angle of roughly 10°. A sketch of both the pixel detector and the silicon strip can be found in Fig. 3.4.
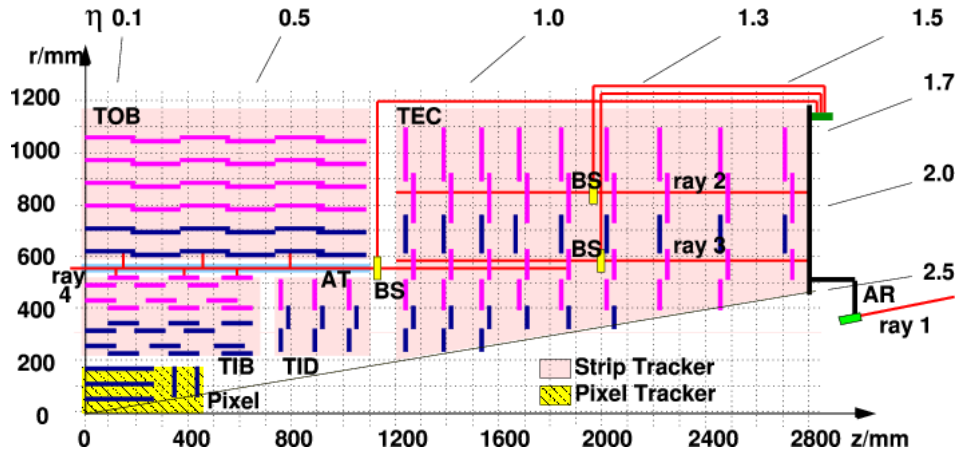

FIGURE 3.4: Sketch of a quarter of all parts in the CMS tracking system with distances in radius *r* and *z*. The pixel detector is close to the interaction point shown in yellow, the silicon strip tracker is underlaid in pink. Each pink and blue solid line represents an active detector layer [7].

Both the FPIX and the BPIX are organized into single detector modules. There are 768 modules in the barrel part and 672 modules in the four forward disks, each consisting of 2 to 16 readout chips (ROCs) [8]. Every ROC has a size of roughly 8×8 mm^2 and is bump-bonded to an active silicon layer of 285 µm in thickness, divided into 52×80 single pixels. In total, there are 1440 modules containing about 16 000 ROCs with a gross pixel count of about 66 million and a total silicon area of about one square meter. Such a high granularity is needed in order to obtain good spacial resolution at the interaction point, good reconstruction of the tracks and in order to keep the occupancy low in high luminosity running of the LHC. At design luminosity of 1×10^{34} m^{-2} s^{-1}, the CMS pixel detector is hit by about 1000 particles per bunch crossing, leading to an occupancy of less than one percent. Even with relatively low occupancies, the total flux of particles in the inner layers of the pixel detector are sufficiently high to induce significant radiation damage. For this reason, the pixel detector has to be replaced during run 2 of the LHC, an event scheduled for late 2017.

The silicon strip tracker

Just outside the pixel detector, further away from the interaction point lies the silicon strip tracker. Its purpose is much the same as the pixel detector, albeit with a much larger covered area and a much smaller number of active channels. It occupies the radial distances from 20 to 116 cm and a length in z-direction of 5.8 m. It is also divided into a cylindrical barrel part and endcap parts perpendicular to the beam direction. The naming scheme of the different parts is the Tracker Inner Barrel (TIB) and the Tracker Outer Barrel (TOB) for the layers parallel to the beam direction and the Tracker Inner Disks (TID) and the Tracker EndCaps (TEC) for the perpendicular part. In total, there are 15 148 single detector modules in the silicon strip tracker[9] with varying sizes of strip widths and inter-strip pitch lengths. The inter strip pitch varies from 80 µm at low radius to 200 µm at higher radius, while the ratio between pitch and width is constant at 0.25. The combined surface of the 9.3 million single channels is around 198 m^2, making it the largest silicon tracker ever built. The thickness of the silicon also varies between 320 µm in the inner part of the detector and 500 µm on the outside part. With this specifications, the total occupancy at design luminosity is approximately 1%. Altogether, a particle traversing the strip tracker will hit about ten active silicon layers[3].

Due to the high granularity, the multi-layered design, and the very high and homogeneous magnetic field in the tracking volume, the performance of the CMS tracking system is impressive. Single point resolutions are around 30 µm and in combination, the impact parameter resolution of is around around 10 µm for high energy muons, while the momentum resolution varies from around 1% for low-p_T muons in the central region to about 8% for high-p_T muons in the forward region.

The electromagnetic calorimeter

CMS has adapted a design with two separate calorimeters for electromagnetically and hadronically interacting particles. Both of those calorimeters are contained within the superconducting magnet, as shown in a sketch of the CMS calorimetry in Fig. 3.5.

The electromagnetic calorimeter (ECAL) is a homogeneous calorimeter made of 68 524 lead tungstate ($PbWO_3$) crystals built to absorb and measure electromagnetically interacting particles such as photons and electrons. The material was chosen for its mechanical and scintillating properties. With a density of 8.28 $kg\,m^{-3}$ it has a very short

---

[3]This depends on the exact trajectory and varies between eight and 14 layers.
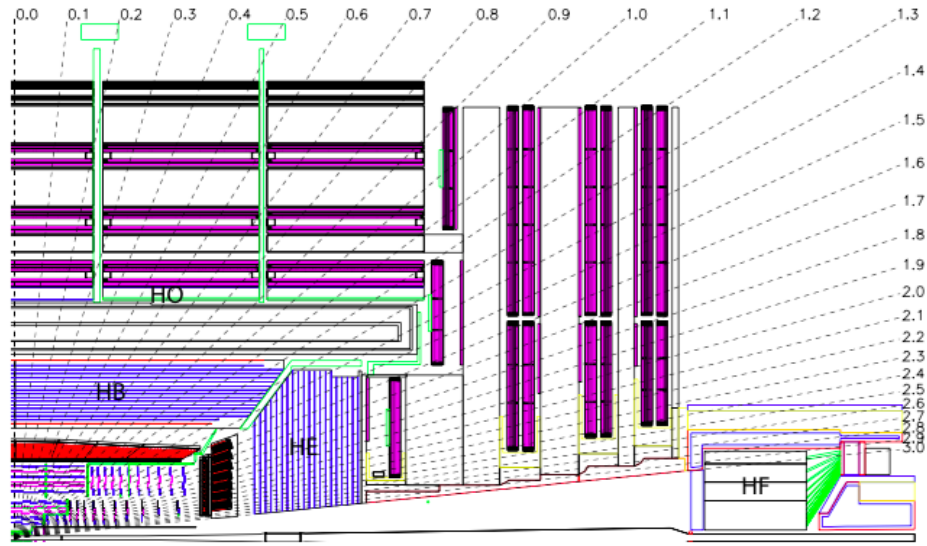
FIGURE 3.5: Design of the CMS calorimetry system. The homogeneous electromagnetic calorimeter is shown in red towards the center of the detector, while the hadronic calorimeter extends to larger radii [4].

radiation length of 0.89 cm as well as a small Molière radius of about 2.2 cm[4] , allowing for a high granularity and adequate spacial resolution of electromagnetic showers. Its scintillating properties include a very short signal collection time of about 25 ns for 80% of the signal and a relatively low photo-electron output of 4.5 per MeVin a wavelength spectrum with a broad maximum in the blue-green 420-430 nm region. This light is collected and amplified by photo-multipliers which are mounted to the rear end of the crystals. Each crystal has an area of 22×22 mm^2 on the front facing side and 26×26 mm^2 on the far side, corresponding to a spacial resolution of 0.0174×0.0174 in η-ϕ. The length in radial direction is 230 mm, corresponding to 25.8 radiation lengths. The barrel part of the ECAL (EB) extends to $|\eta|$ = 1.479, and the endcap part (EE) covers the pseudorapidity range from 1.479 $< |\eta| <$ 3.0.

The energy resolution of a calorimeter can be parametrized by

$$\left(\frac{\sigma}{E}\right) = \left(\frac{a}{\sqrt{E}}\right) \oplus \left(\frac{b}{E}\right) \oplus c, \tag{3.3}$$

where a is called the stochastic term, b the noise term, and c a constant term. At low particle energies both the stochastic term and the noise term dominate the resolution, while at higher energies the importance of the constant term becomes more important. From measurements in testbeams, the terms for the energy resolution of the CMS ECAL

---

[4]The radiation length is the distance at which the energy of an incoming electron has decreased to $\frac{1}{e} \sim$37% due to bremsstrahlung and about $\frac{7}{9}$ times the distance after which a high energy photon would produce an e^+e^- pair. The Molière radius defines the transverse containment of an electromagnetic shower.

were found to be

$$a = 2.8\%,$$
$$b = 12.0\%,$$
$$c = 0.3\%,$$

for the energy in GeV [10]. For the most relevant physical processes, such as $H \to \gamma\gamma$ or $Z \to e^+e^-$, the total resolution both for electrons and photons is of the order of 1% in the central part and of the order of a few percent in the forward part of the detector.

The hadronic calorimeter

For an accurate measurement of the missing transverse energy or momentum, a precise knowledge of the energy of hadronic jets is of paramount importance. However, since the available volume within the CMS magnet is limited, a compromise on the hadronic calorimeter (HCAL) had to be made. The implemented design is a sampling calorimeter, interleaved layers of a massive passive absorber material and a lighter, but active scintillating material. The task of the passive absorber is to create particle showers, which can then be measured in the active material.

The geometry is again divided into a barrel (HB) and an endcap (HE) part. The HB consists of two steel plates as first and last absorber layer and 14 layers of brass of variable thickness in between. In total, these 16 layers of absorber material in the barrel amount to 5.82 interaction lengths [5] of material at $\eta = 0$ up to 10.6 interaction lengths at $|\eta| = 1.3$. The HE is composed of 18 brass absorber plates constituting about 10 interaction lengths along the coverage up to $|\eta| = 3.0$. Every absorber plate is combined with a layer of plastic scintillator organized in tiles each occupying an area of 0.087×0.087, which drives the spacial resolution of the hadronic calorimeter. In addition to the components contained within the superconducting magnet, the hadronic calorimeter features another layer of detector material just outside the magnet, called the hadronic outer (HO) in order to measure hadronic jets with an energy sufficient to traverse the HB and the magnet (so-called punch-throughs). There is also a hadronic calorimeter for high-η jets, called the hadronic forward (HF) covering pseudo-rapidities of $3.0 < |\eta| < 5.0$.

Since the HCAL is a sampling, rather than a homogeneous, calorimeter involving large parts of inactive material, its energy resolution is significantly worse than the one of the ECAL. Adding to this lower precision is the fact that hadronic interactions are accompanied by some unmeasurable energy losses in nuclear excitations. Using the same

---

[5]An interaction length corresponds to the mean distance at which a hadronic particle undergoes a nuclear interaction.

parametrization as in Eq. 3.3, the parameters for the HCAL are found to be

$$a = 1.25,$$
$$b = 5.6,$$
$$c = 0.033.$$

For relevant hadronic jets in analyses for SUSY and most other use-cases, the resolution takes values of about 25 % for 40 GeV jets and decreases with energy to values of about 10 % or less at energies of jets above 100 GeV.

The muon system

As the acronym CMS already suggests, special emphasis in the design of the detector was put into designing and constructing a system which is capable of measuring muons with a very high precision in order to be sensitive to high-sensitivity processes such as the Higgs boson decaying into four leptons. This is achieved by three types of gaseous detectors encased in the return yoke of the magnet, namely the Drift Tubes (DTs) in the barrel part, Cathode Strip Chambers (CSCs) in the two endcap parts, and a set of fast Resistive Plate Chambers (RPCs) used for triggering on muons and timing. The total coverage can be expressed by the reconstruction efficiency as a function of the pseudo-rapidity, which achieves values close to 100 % all from values of $0. < |\eta| < 245$, with a notable exception at around $|\eta| = 0.25$, and $|\eta| = 0.8$, where it drops to around 94 % and 97 %, respectively, due to small gaps between the DTs. The layout of the muon system can be seen in Fig. 3.6, where a quadrant of the CMS detector is shown.

The DTs are organized in four concentrical cylinders in the barrel part with a total of 250 drift chambers containing 172 000 active wires. They are made of multiple so-called superlayers, which are essentially stacked tubes either in beam direction or perpendicular to it. Two or three of those superlayers are then combined into one DT, with altering orientation of the wires to provide maximum spacial resolution. RPCs are glued to the DTs, on both sides for the inner two cylinders and on the inner side for the outer two. The gas in the drift tubes is a mixture of 85% Ar and 15% CO_2 and the drift length is chosen to be 21 mm with a drift time of roughly 380 ns, allowing for negligible occupancy.

Because of the much higher flux and an inhomogeneous magnetic field in the forward part of the detector, a different detector design had to be chosen for high values of $|\eta|$. The CSCs are a set of 468 trapezoidal modules, each covering from $10°$ to $20°$ in ϕ. Each CSC consists of six gas-filled gaps with cathode strips running radially and anode wires
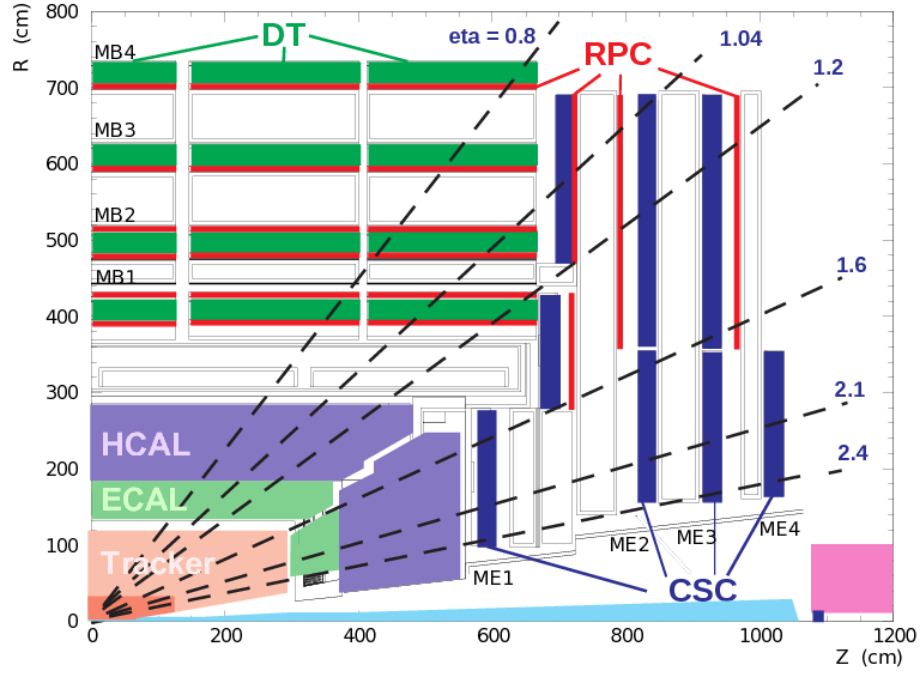
FIGURE 3.6: Layout of the CMS muon system. The DTs comprise the barrel part of the detector, while the CSCs are exclusively situated in the endcap part. RPCs are attached to both types of detectors for triggering and timing measurements [11].

running almost perpendicular to the strips. The r, ϕ, and z coordinates of a traversing muon is thus measured six times per CSC, and there are in total four layers of CSCs in each endcap. There are a total of 220 000 readout channels of the strips and another 180 000 readout channels of the wires, allowing for good spacial resolution and low occupancy even at high flux rates of up to $1\,\mathrm{kHz\,cm^{-2}}$ at full LHC luminosity. The gas mixture is 40% Ar, 50% CO_2, and 10% CF_4, where the CO_2 component achieves a high signal gain, while the CF_4 component protects the wires from polymerisation. Three layers of RPCs are connected to the CSCs in the outer part of the endcap.

RPCs are gas-filled detectors which have a very fast signal rise-time, comparable to that of scintillators. Since the time resolution is much better than the LHC bunch spacing of 25 ns, the RPCs provide not only an accurate estimate of the momentum of a muon, but also unambiguous assignment to a bunch crossing. Each RPC is made up of two 2 mm wide, gas-filled gaps with strips on the common side and plates of plastic on the outer sides. These simple circuits are operated in avalanche mode in order to ensure good operation at high rates.

Using the three muon-subsystems and combining their measurement, a standalone muon momentum resolution of below 10% can be achieved for muons up to 200 GeV.

This value increases to between 15% and 40% for muons of 1 TeV momentum, depending on the position in $|\eta|$. Since a muon can be identified also in the tracker volume, combining the tracks from the inner part of the detector with the information of the muon chambers improves this resolution to roughly a percent for momenta below 200 GeV and about 5% for momenta of 1 TeV.

Chapter 4

Event reconstruction and simulation

The basic quantity for readout, reconstruction, and further processing as well as data analysis is called the 'Event' and refers to a full readout of the CMS detector. This chapter explains the various steps leading from an actual physical bunch crossing with proton-proton collisions taking place within CMS to a reconstructed event which can be used for data analysis. First, a sequence of data reduction has to take place in order to cope with the stupendous amount of data produced by the CMS detector. Secondly, the binary data coming out of the electronics has to be combined into a physical picture of a collision or an event using specifically designed software frameworks and reconstruction code. Lastly, this chapter also gives a short overview on how physics processes can be simulated and how this can be combined with a simulated version of the CMS detector for the production of background and signal data samples which are then used for the ensuing data analysis.

4.1   The trigger system

With a bunch crossing frequency of 40 MHz and a mean number of collisions per bunch crossing of roughly 20, there are of the order of 800 million collisions taking place inside CMS every second. Considering that the whole of CMS has roughly 100 million readout channels, this would lead to unsustainable data-rates, even for the most powerful readout and network possible to date. For this reason, a triggering system has been implemented in order to differentiate 'interesting' collisions from those who are considered not. CMS has adopted a two-stage approach, with a first, hardware-based and thus very fast triggering mechanism called the Level-1 trigger (L1), followed by a second, fully software based trigger named the High-Level-Trigger (HLT).

4.1.1 The L1 trigger

Dealing with complicated data at a rate of 40 MHz requires for processing of information at speeds that are unattainable for software reconstruction. Therefore, a fully hardware based system has been implemented, relying heavily on the use of integrated circuits in the form of so-called Field-Programmable-Gate-Arrays (FPGAs). Because speed is such an important point of the triggering decision, not all information from the detector can be used in order to make a yes/no decision on an event-by-event basis. In the current L1 trigger system, only coarsely segmented information from the calorimeters and the muon system are used for the trigger decision, while the full data from the muon system, the calorimeter, and the silicon tracker are stored in buffers until a trigger accept (L1 accept) triggers the full readout of these buffers. An organizational sketch of the different participants for a trigger decision is shown in Fig. 4.1 The
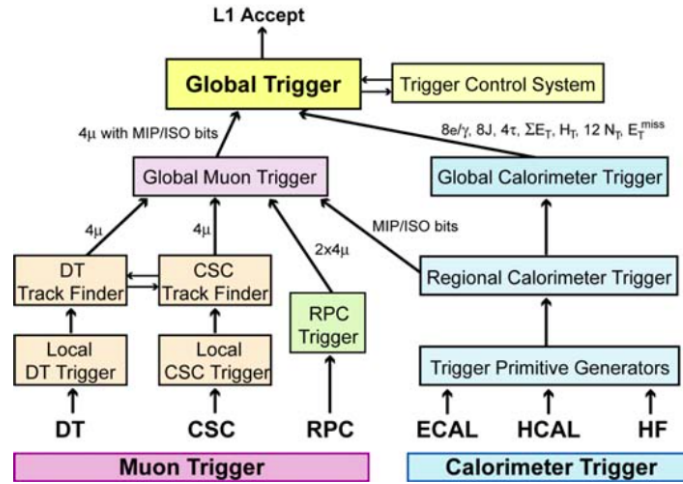

FIGURE 4.1: Organizational chart of the various components of any L1-accept. The two systems (calorimetry and muons) work in parallel until they are combined at a regional/global level into the global trigger decision [4].

calorimeter part of the trigger has inputs from the ECAL, HCAL, and the HF, constructing first so-called Trigger Primitives from coarsely organized trigger 'towers'. These are then fed into a regional trigger, where energy sums and crude identifications of physical objects are performed. This information is then given to the global trigger, which constructs relevant variables such as the total energy deposited, the number of jets, etc. In parallel, the muon system tries to identify tracks of muons and calculate their p_T by taking information from all three sub-systems and combining it into the Global Muon trigger. This output is then combined with the calorimeter trigger into a final trigger decision, the aforementioned L1-accept.

The input rate to the L1 is the bunch crossing frequency of the LHC and the maximum processing time of the L1 logic is 3.2 µs. The output rate, i.e. the rate of L1-accepts, is

limited to 100 kHz. At this rate, the L1-accept is passed to all the subdetectors, triggering full readout of the event information stored in buffers. This set of complete data is then passed on to the HLT.

4.1.2 The HLT

At the L1 output rate, the full information from the detector is sent from the experimental cavern at P5 to a computer farm situated above ground for further processing. This computer farm is made of a large number of commercial CPUs (in total about 13 000) cores, running reconstruction software which is implemented into the whole CMS reconstruction software, package described below in section **??**, albeit with different sets of parameters optimized for speed [12, 13]. The HLT starts with L1 information on the candidates for physical objects, and improves the reconstruction. The organization is done in so-called HLT paths, which are essentially requirements on physical objects being present in a collision. An example which will be used later on in the analysis part of this thesis is `HLT_Mu17_Mu8_v1`, which requires the presence of one muon with p_T greater than 17 GeVand another muon with p_T greater than 8 GeVon HLT level. Other 'online' physical objects in the HLT include electrons, jets, missing transverse energy, and H_T – the scalar sum of all jet-p_Ts above a threshold. The reconstruction of objects is divided into modules for any given quantity, followed by a filter on the quantity where a cut is applied, in order to save precious computation time of unnecessary quantities. The largest fraction of computation time is taken up by the tracking, and the total time required for an event depends on the exact event kinematics, up to a limit of 200 ms.

The total data reduction factor of the HLT system is roughly 10×10^2, so the final output rate of events actually fully reconstructed and saved on hard-drives is of the order of 1 kHz. About half of this data is reconstructed in the immediate time period after the collision, whereas the other half of the data is first stored and reconstructed only later, when computing resources for reconstruction are freed. This process is called data-parking and was implemented for the first time in 2012.

To facilitate analysis of the data when it is fully reconstructed after passing the HLT, different HLT paths are organized in various so-called primary datasets (PDs), which group similar events into one collection. Examples for primary datasets are DoubleMu, DoubleElectron, and MuEG.

4.2   Reconstruction and data formats

Upon passing the HLT at P5, collision data are sent to the CERN Tier-0 computing center located at the CERN main site in Meyrin for full reconstruction at a rate of roughly 1 kHz. Full reconstruction of each triggered event is then performed by the CMS software framework called CMSSW (FIXME cite). For data analysis it is necessary to obtain a data format in which physical objects can be identified, this is called the *Event Data Model*, EDM. CMSSW reconstructs different detector related quantities such as calorimeter energy deposits, tracks from the pixel and strip tracker and muons from the muon chambers, with the best available precision and places those objects into the EDM. It also combines those quantities into physical particles and observables as described below.

Tracks are reconstructed using an iterative tracking algorithm where in a first iteration tight criteria for track-seeding are used in order to minimize reconstruction of fake tracks. In subsequent iterations the set of previously found tracks are used as input, loosening the track fitting requirements to regain tracking efficiency. Five iterations are done, leading to efficiencies of about 99.5% for muons, and well above 90% for charged hadrons within the tracker volume. Tracks with as little as three hits in the 10 layer tracker can be reconstructed, with a minimal transverse momentum of about 150 MeV, while the fake rate is kept to below one percent [**?**].

Calorimeter clusters are reconstructed by searching for calorimeter cells with an energy deposit above a certain seed-threshold. These are then combined with adjacent cells beyond a threshold equivalent to about twice the electronic noise (80-300 MeVin the ECAL and 800 MeVin the HCAL).

Subsequently, these detector-based objects are combined through an algorithm called 'Particle Flow' (PF) to identify candidates for physical objects.

4.2.1   Particle flow

The particle flow algorithm [14] aims at reconstructing an integral picture of every triggered bunch crossing by combining information from all subdetectors to identify PF candidates. These are photons, electrons, muons, neutral hadrons, and charged hadrons.

First, tracks are combined with the information from the muon chambers to search for 'global muons' which have both a track, and are reconstructed in the muon system. If a match is found, this PF muon is put into the appropriate collection in the EDM and the

track is removed from the collection of tracks. The second step involves the matching of tracks and energy clusters in the ECAL, producing a candidate electron. These are then refit with a Gaussian Sum Filter (GSF) in order to account for bremsstrahlung on the electrons trajectory and the tracks are removed from the track collection. Remaining tracks are then matched to HCAL deposits to construct a collection of charged hadrons. Any energy deposit that does not have an associated track, is then interpreted as a photon or a neutral hadron, depending on the energy fractions in the ECAL and HCAL.

The PF candidates obtained by this algorithm are then taken as the input to the clustering algorithm of hadronic jets. This jet clustering algorithm most widely used in CMS is the so-called anti-k_T clustering algorithm [15], developed in 2008. This algorithm is both collinear, and infrared safe[1] and the distance parameters of the clustering algorithm are

$$d_{ij} = \min\left(k_{T,i}^{-2}, k_{T,j}^{-2}\right) \frac{(\Delta R)_{ij}^2}{R^2}, \tag{4.1}$$

$$d_{iB} = k_{T,i}^{-2}, \tag{4.2}$$

$$d_{jB} = k_{T,j}^{-2}. \tag{4.3}$$

In this equation, R defines the radial size of a jet, ΔR is the spacial distance between two candidate particles i and j, while $k_{T,i}$ and $k_{T,j}$ are the transverse momenta of particles i and j. If the minimum distance is either d_{iB} or d_{jB}, the particle is called a jet and is removed from the collection. Whereas if the minimum distance is d_{ij}, the two particles i and j are merged into a new particle. Because of the inverse exponent in the minimum of the two transverse momenta squared, this means that the anti-k_T algorithm clusters soft particles around the hard particles before clustering of soft particles among each other takes place. This leads to perfectly circular jets (as long as they do not overlap), facilitating corrections to be made due to pileup and other effects.

It is worthwhile to note here, that the PF algorithm in combination with the jet clustering produces overlaps between physical objects. As an example, a muon can enter both the muon collection and can be reconstructed as a jet. It is therefore important to employ some cross-cleaning of objects in any analysis.

---

[1]Collinear safety describes invariance of a jet's properties upon division of a constituent's energy into two collinear particles. Infrared safety refers to invariance of the jet upon addition of very soft, i.e. low-energetic, particles

4.2.2 Data formats

Centrally reconstructed events are saved in various data formats all based on EDM, but with differing detail of content. The basic format is RAW, which stored the raw detector information. Output from the full reconstruction at the Tier-0 is saved in the RECO data format. This format allows for much flexibility, albeit at very large event sizes, rendering it impractical for daily use. The most used format for processing in data analyses is called AOD, Analysis Object Data. This is a simple subset of the RECO data format, containing all relevant information for data analysis. The event size of one RECO event is about 1.2 MB, while AOD events are of the order of 300 kB, depending on the kinematics of the event.

Each event is saved at least twice, one copy usually lying at the CERN Tier-0 computing center, and another copy distributed in the LHC Computing Grid (LCG), a worldwide network of computer centers for data analysis and storage. Analysis of the data is done with user-written programs running on AOD events. Since primary datasets are of significant size containing oftentimes many million events at once, these programs are sent by the user via the LCG to a computing center which hosts the dataset of interest, rather than the dataset being copied to the user. The final data formats used in small-scale analysis are ROOT based files [16]. ROOT is a data analysis framework conceived especially for data analysis at CERN. It features many convenient data formats, such as TTrees[2], and provides capabilities of producing plots, histograms, perform fits and many more functionalities.

4.3 Simulation and Monte-Carlo

For a number of different reasons, it is necessary to be able to simulate physical processes from theoretical models such as the Standard Model or Supersymmetry and feeding them into a simulation of the CMS detector. These reasons include testing the behavior of the CMS detector, validation of known physical processes, background studies for searches for new physics, signal studies for physics searches and many more. Complete simulation of a physics event in CMS is a very complicated and multi-layered process. It starts from the actual physical process from calculations with matrix elements, continues with the decay of the produced particles including hadronization of quarks and radiations during this process. Once a 'stable' physical process is generated, the interaction with the simulated version of the CMS detector has to be implemented in order to end up with a set of binary data similar to what comes out of

---

[2]See `http://root.cern.ch/root/html/TTree.html` for more details.

regular data-taking. Once this step is achieved, the reconstruction software described in Section 4.2 processes these data in the exact same way as collision events. This section gives a quick overview of all the steps involved and software packages capable of performing these different tasks.

4.3.1 Simulation of hard parton scattering

The underlying physical theories and mathematical framework of how to simulate and calculate scattering amplitudes was already described in section XX FIXME, however an implementation of these complicated calculations will be discussed here. There are a number of tools on the market for this step of event simulation, which differ most notably in the order of the perturbative expansion in the strong coupling constant, α_s. They are all summarized as so-called Monte-Carlo (MC) generators, as they make heavy use of the Monte-Carlo method of random sampling of distributions.

Parton distribution functions

One important piece of input to calculate a hard parton scattering amplitude are the so-called parton distribution functions, PDFs. They describe at a given energy of the proton-proton collision the probabilities of finding a given type of parton, gluons and (anti-)quarks, at a certain energy fraction x of the proton. An example for PDFs from the MRST/MSTW collaboration can be seen in Fig. 4.2. The red curve in Fig. 4.2 represents the gluon PDF, which is divided by a factor 10 in order to fit the scale, while the others are for quarks and anti-quarks. It is easy to see from these graphs, that overall parton-parton interactions at the LHC are dominated by relatively low-energy gluon induced processes. Only processes which require a large invariant mass (i.e. large values of x for both partons) are dominated by valence-quark induced processes. PDFs are measured by performing fits to a wide range of kinematic distributions from collider experiments, especially from deep inelastic electron-proton scattering. Alongside the commonly used MRST/MSTW PDF sets, there are others used within CMS such as CTEQ, and NNPDF [17, 18].

Hard scattering generators

As briefly stated before, there are many different implementations of calculating the matrix element (ME) part of a hard partonic scattering. The main difference being the order of α_s in which this calculation is done. Since higher order calculations are generally expected to give a better description of the process, higher order matrix element
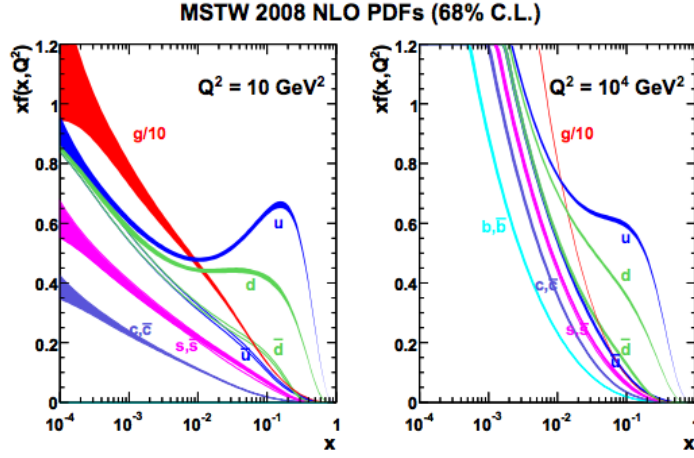
FIGURE 4.2: Parton distribution functions of the proton for two different resolution scales Q^2. This particular set of parton distribution functions is obtained from the MRST/MSTW collaborations [19].

generators are considered more accurate. The most commonly used leading order (LO) matrix element generator is MadGraph[20], it not only does the leading order matrix element calculations, but also includes the real corrections of the next-to-leading order contribution, while the virtual corrections are unaccounted for. Most simulated samples used in the data analysis section of this thesis use MadGraph in version FIXME. An example of a fully next-to-leading order (NLO) matrix element generator is POWHEG [21], capable of calculating MEs of most relevant processes at the LHC. Recently, the MadGraph ME generator has been combined with an NLO generator called MC@NLO [22] into a common package called MadGraph5_aMC@NLO[3], which will play a crucial role in future data analyses [23]. In addition to the ME generators, there is a set of widely used multi-purpose event generators that do not specifically calculate the matrix element, but rather use libraries of processes in order to simulate events. Examples for such more phenomenological event simulators used at CMS are PYTHIA and HERWIG [24, 25]. All the aforementioned generators do not only provide simulated events in the form of text-based files with the four-momenta of all the simulated particles, but they also give a value for the cross-section of each process, which can then be used as a normalization to the data.

4.3.2 Decays, hadronization, and radiations

After the generation of the hard scattering process, the produced particles have to be decayed in the case of non-stable particles, hadronized in the case of quarks in the final state, and appropriate radiations in both the initial-, and final state have to be added

---

[3]Creativity in name-finding was not given highest priority in the development of this project.

to the event. The decay of unstable particles is somewhat arbitrarily taken care of by the ME generator for particles with a short lifetime, such as W and Z bosons, while longer living particles are usually decayed by the parton showering part described just below. There also exist a few specific decay simulators in order to preserve proper spin-information in the decay of τ leptons and heavy resonances, named `Tauola` and `MadSpin`, respectively [26, 27].

Since the hadronization of quarks and gluons into hadronic jets is an extremely challenging task to describe in perturbative QCD as it involves a large number of strong interactions [4] no attempt is made to calculate these steps one by one. Rather, a phenomenological approach is taken in order to describe measured data. This step is therefore performed by the multi-purpose event generators such as `PYTHIA` and `HERWIG` by employing underlying simplified models and tuning their parameters to the measured data for maximum data-MC consistency.

Initial and final state radiation is also added by the multi-purpose event generators. An added complication of the simulation of initial and final state radiation is the matter of phase-space matching. For instance, if events are generated at LO+NLO by a ME generator and then passed over to `PYTHIA` or `HERWIG` for further processing, the possibility of adding a final state radiated gluon in a phase space region that is already covered by the NLO simulation of the event has to be taken into account. For this reason matching algorithms have to be employed at this stage.

4.3.3 Detector simulation

Once all these issues with the generation of a set of stable particles are taken care of by the different MC generators, one is left with a large number of particles that interact with the detector and give electronic signals in the many readout channels of CMS. This task is performed by a software package called `GEANT4` [28]. A very detailed software model of the CMS detector is implemented in `GEANT4` and all particle-detector interactions such as ionization, multiple scattering and nuclear interactions are simulated from large libraries. The signal output of all the channels is then generated and saved in an EDM format identical to that of actual collision data. This EDM is then treated in the exact same way for reconstruction, clustering and further analysis as collision data. The full simulation of all interactions is a very computing intensive task with a computing time of about one minute per event, depending on the number of final state particles. For this reason, a faster simulation package has been developed which

---

[4]There are processes for which it is outright impossible to use perturbative QCD to describe this, such as bound states of quard-anti-quark pairs.

parametrizes the interactions, leading to much reduced computing time of the order of seconds per event. There are therefore two types of simulated datasets, FULLSIM and FASTSIM [29]. The difference between the two types of simulation have to be taken into account on the analysis level.

4.4   Datasets used for analysis

Chapter 5

Same-sign dilepton analyses

5.1   Search for Supersymmetry in events with hadronic activity

5.2   Search for electroweak production of Supersymmetry

5.3   Fake leptons

Chapter 6

Outlook

Chapter 7

Conclusions

Appendix A

Dummy Appendix

You can defer lengthy calculations that would otherwise only interrupt the flow of your thesis to an appendix.

List of Figures

List of Tables

Abbreviations

LAH List Abbreviations Here

Symbols

a	distance	m
P	power	W (Js^{-1})
ω	angular frequency	rads^{-1}

Bibliography

[1] Oliver Sim Brüning, Paul Collier, P Lebrun, Stephen Myers, Ranko Ostojic, John Poole, and Paul Proudlock. *LHC Design Report*. CERN, Geneva, 2004.

[2] The UA1 collaboration. *Experimental observation of isolated large transverse energy electrons with associated missing energy at s=540 GeV*. *Physics Letters B*, 122(1):103 – 116, 1983. ISSN 0370-2693. doi: http://dx.doi.org/10.1016/0370-2693(83)91177-2. URL http://www.sciencedirect.com/science/article/pii/0370269383911772.

[3] The UA1 collaboration. *Experimental observation of lepton pairs of invariant mass around 95 GeV/c² at the CERN SPS collider*. *Physics Letters B*, 126(5):398 – 410, 1983. ISSN 0370-2693. doi: http://dx.doi.org/10.1016/0370-2693(83)90188-0. URL http://www.sciencedirect.com/science/article/pii/0370269383901880.

[4] R. Adolphi et al. The CMS experiment at the CERN LHC. *JINST*, 3:S08004, 2008. doi: 10.1088/1748-0221/3/08/S08004.

[5] The CMS Collaboration. Public CMS luminosity information, 2014. URL https://twiki.cern.ch/twiki/bin/view/CMSPublic/LumiPublicResults#Pileup_distribution.

[6] *The CMS magnet project: Technical Design Report*. Technical Design Report CMS. CERN, Geneva, 1997.

[7] W. Adam et al. Alignment of the CMS Silicon Strip Tracker during stand-alone Commissioning. *JINST*, 4:T07001, 2009. doi: 10.1088/1748-0221/4/07/T07001.

[8] D. Kotliński, E. Bartz, W. Erdmann, K. Gabathuler, R. Horisberger, Ch. Hörmann, H-Ch. Kästli, B. Meier, and S. Schnetzer. The control and readout systems of the CMS pixel barrel detector. *Nuclear Instruments and Methods in Physics*

Research Section A: Accelerators, Spectrometers, Detectors and Associated Equipment, 565(1):73 – 78, 2006. ISSN 0168-9002. doi: http://dx.doi.org/10.1016/j.nima.2006.04.065. URL http://www.sciencedirect.com/science/article/pii/S0168900206007200. Proceedings of the International Workshop on Semiconductor Pixel Detectors for Particles and Imaging PIXEL 2005 International Workshop on Semiconductor Pixel Detectors for Particles and Imaging.

[9] Paolo Azzurri. The CMS silicon strip tracker. *J.Phys.Conf.Ser.*, 41:127–134, 2006. doi: 10.1088/1742-6596/41/1/011.

[10] The CMS Collaboration. Energy calibration and resolution of the CMS electromagnetic calorimeter in pp collisions at $\sqrt{s}$ = 7 TeV. *Journal of Instrumentation*, 8 (09):P09009, 2013. URL http://stacks.iop.org/1748-0221/8/i=09/a=P09009.

[11] Min Suk Kim et al. CMS reconstruction improvement for the muon tracking by the RPC chambers. *PoS*, RPC2012:045, 2012. doi: 10.1088/1748-0221/8/03/T03001.

[12] Valentina Gori. The CMS High Level Trigger. *Int.J.Mod.Phys.Conf.Ser.*, 31:1460297, 2014. doi: 10.1142/S201019451460297X.

[13] Daniele Trocino. The CMS High Level Trigger. *J.Phys.Conf.Ser.*, 513:012036, 2014. doi: 10.1088/1742-6596/513/1/012036.

[14] Particle-Flow Event Reconstruction in CMS and Performance for Jets, Taus, and MET. Technical Report CMS-PAS-PFT-09-001, CERN, 2009. Geneva, Apr 2009.

[15] Matteo Cacciari, Gavin P. Salam, and Gregory Soyez. The anti- k t jet clustering algorithm. *Journal of High Energy Physics*, 2008(04):063, 2008. URL http://stacks.iop.org/1126-6708/2008/i=04/a=063.

[16] ROOT - An Object Oriented Data Analysis Framework, Sep. 1997. http://root.cern.ch/.

[17] Richard D. Ball, Valerio Bertone, Stefano Carrazza, Christopher S. Deans, Luigi Del Debbio, et al. Parton distributions with LHC data. *Nucl.Phys.*, B867:244–289, 2013. doi: 10.1016/j.nuclphysb.2012.10.003.

[18] J.F. Owens, A. Accardi, and W. Melnitchouk. Global parton distributions with nuclear and finite-Q^2 corrections. *Phys.Rev.*, D87(9):094012, 2013. doi: 10.1103/PhysRevD.87.094012.

[19] A.D. Martin, W.J. Stirling, R.S. Thorne, and G. Watt. Parton distributions for the LHC. *Eur.Phys.J.*, C63:189–285, 2009. doi: 10.1140/epjc/s10052-009-1072-5.

[20] Stefano Frixione and Bryan R. Webber. Matching NLO QCD computations and parton shower simulations. *JHEP*, 0206:029, 2002. doi: 10.1088/1126-6708/2002/06/029.

[21] Stefano Frixione, Paolo Nason, and Carlo Oleari. Matching NLO QCD computations with Parton Shower simulations: the POWHEG method. *JHEP*, 0711:070, 2007. doi: 10.1088/1126-6708/2007/11/070.

[22] Stefano Frixione, Fabian Stoeckli, Paolo Torrielli, Bryan R. Webber, and Chris D. White. The MCaNLO 4.0 Event Generator. 2010.

[23] J. Alwall, R. Frederix, S. Frixione, V. Hirschi, F. Maltoni, et al. The automated computation of tree-level and next-to-leading order differential cross sections, and their matching to parton shower simulations. *JHEP*, 1407:079, 2014. doi: 10.1007/JHEP07(2014)079.

[24] Torbjorn Sjostrand, Stephen Mrenna, and Peter Z. Skands. PYTHIA 6.4 Physics and Manual. *JHEP*, 0605:026, 2006. doi: 10.1088/1126-6708/2006/05/026.

[25] Stefan Gieseke, Alberto Ribon, Michael H Seymour, P. Stephens, and Bryan Webber. Herwig++ 1.0: An Event generator for e+ e- annihilation. *JHEP*, 0402:005, 2004. doi: 10.1088/1126-6708/2004/02/005.

[26] Stanislaw Jadach, Johann H. Kuhn, and Zbigniew Was. TAUOLA: A Library of Monte Carlo programs to simulate decays of polarized tau leptons. *Comput.Phys.Commun.*, 64:275–299, 1990. doi: 10.1016/0010-4655(91)90038-M.

[27] Pierre Artoisenet, Rikkert Frederix, Olivier Mattelaer, and Robbert Rietkerk. Automatic spin-entangled decays of heavy resonances in Monte Carlo simulations. *JHEP*, 1303:015, 2013. doi: 10.1007/JHEP03(2013)015.

[28] S. Agostinelli et al. GEANT4: A Simulation toolkit. *Nucl.Instrum.Meth.*, A506:250–303, 2003. doi: 10.1016/S0168-9002(03)01368-8.

[29] S Abdullin, P Azzi, F Beaudette, P Janot, A Perrotta, and the CMS Collaboration. The fast simulation of the cms detector at lhc. *Journal of Physics: Conference Series*, 331(3):032049, 2011. URL http://stacks.iop.org/1742-6596/331/i=3/a=032049.

Acknowledgements

The acknowledgements and the people to thank go here, don't forget to include your project advisor...